GEOPHYSICS, VOL. 74, NO. 5 (SEPTEMBER-OCTOBER 2009); P. R85–R97, 16 FIGS.
10.1190/1.3190131

Ray-based stochastic inversion of prestack seismic data for improved reservoir characterization

Dennis van der Burg[1], Arie Verdel[2], and Kees Wapenaar[3]

ABSTRACT

Trace inversion for reservoir parameters is affected by angle averaging of seismic data and wavelet distortion on the migration image. In an alternative approach to stochastic trace inversion, the data are inverted prestack before migration using 3D dynamic ray tracing. This choice makes it possible to interweave trace inversion with Kirchhoff migration. The new method, called ray-based stochastic inversion, is a generalization of current amplitude versus offset/amplitude versus angle (AVO/AVA) inversion techniques. The new method outperforms standard stochastic inversion techniques in cases of reservoir parameter estimation in a structurally complex subsurface with substantial lateral velocity variations and significant reflector dips. A simplification of the method inverts the normal-incidence response from reservoirs with approximately planar layering at the subsurface target locations selected for inversion. It operates along raypaths perpendicular to the reflectors, the direction that offers optimal resolution to discern layering in a reservoir. In a test on field data from the Gulf of Mexico, reservoir parameter estimates obtained with the simplified method, the estimates found by conventional stochastic inversion, and the actual values at a well drilled after the inversion are compared. Although the new method uses only 2% of the prestack data, the result indicates it improves accuracy on the dipping part of the reservoir, where conventional stochastic inversion suffers from wavelet stretch caused by migration.

INTRODUCTION

Techniques that invert seismic data can be used to estimate rock and pore-fluid properties of oil and gas reservoirs in the subsurface. With inversion, detailed information about a reservoir that is available at well locations is extrapolated away from the wells to all locations in the reservoir on the basis of seismic reflections. Examples of reservoir properties that can be inverted for are thickness, wave propagation velocity, porosity, and pore-fluid type of individual layers. The initial layered reservoir model is derived from well-log data, seismic reflection picks, and geologic information. The wavelet required for inversion is derived from a seismic-to-well match (White and Simm, 2003). For a recent overview of inversion techniques, see Veeken and Da Silva (2004).

Stochastic trace inversion is a generic term for a specific subset of trace inversion techniques that quantifies uncertainties in reservoir-parameter estimates. This is achieved by applying Bayes' rule (Duijndam, 1987; Leguijt, 2001; Tarantola, 2005). Consequently, the method also requires initial uncertainty estimates of all model parameters based on prior knowledge. In Bayesian inversion, forward modeling a trace from the migration image and the subsequent comparison of modeled and actual trace is done many times to evaluate the uncertainties in the reservoir parameters. This procedure is repeated for every trace in the inversion range. A Markov-chain Monte Carlo algorithm (Sambridge and Mosegaard, 2002) can be used to generate parameter updates to efficiently sample the posterior probability density function (PDF) in a statistically valid way. The method is a global optimization technique. Local optimization techniques such as conjugate gradient often have difficulties because they cannot escape local extremes that might be present in the corresponding posterior PDF.

The forward-modeling stage in conventional trace inversion is depicted in greater detail in the process flow at the bottom of Figure 1. Initial estimates of rock and pore-fluid properties acquired from the layered reservoir model at the current trace position are inserted into 1D rock/fluid property models appropriate for each identified layer in the inversion target. Using these rock models, the elastic-layer

Manuscript received by the Editor 24 November 2008; revised manuscript received 27 February 2009; published online 18 September 2009.
[1]Formerly Delft University of Technology, Delft, The Netherlands; presently Petroleum Geo-Services B. V., Leiden, The Netherlands. E-mail: dennis.van.der.berg@pgs.com.
[2]Shell International Exploration and Production B.V., Rijswijk, The Netherlands. E-mail: arie.verdel@shell.com.
[3]Delft University of Technology, Department of Geotechnology, Delft, The Netherlands. E-mail: c.p.a.wapenaar@tudelft.nl.
© 2009 Society of Exploration Geophysicists. All rights reserved.

Downloaded 21 Sep 2009 to 145.94.65.141. Redistribution subject to SEG license or copyright; see Terms of Use at http://segdl.org/

properties — P-wave velocity V_P, S-wave velocity V_S, and density ρ are calculated. Subsequently, using the Zoeppritz equations (given in, e.g., Young and Braile, 1976), the reflection coefficients $R(\theta)$ at each layer interface are calculated as a function of angle of incidence θ, locally assuming a 1D layered earth. With thicknesses from the initial layered reservoir model, a spiky reflectivity trace $r(t)$ is built and convolved with a wavelet from a seismic-to-well tie to create the modeled trace.

PROBLEMS WITH TRADITIONAL STOCHASTIC INVERSION

For the scheme displayed in Figure 1, 1D convolution is used to model traces in the migrated domain (Oldenburg et al., 1983; van Riel and Berkhout, 1985), i.e.,

$$s(t) = w(t) * r(t), \tag{1}$$

in which the asterisk denotes temporal convolution, $s(t)$ is the modeled seismic trace, $w(t)$ is the wavelet, and $r(t)$ is the subsurface spiky reflectivity — the impulse response of a 1D layered earth for primary unconverted reflected waves.

Because inversion is an iterative procedure, the forward modeling must be computationally fast, justifying the choice for 1D convolution. However, with the increased computing power available today, a more sophisticated forward modeler should be considered to remove some of the limitations of 1D convolution. For example, 1D convolution does not take into account that the image has a lateral resolution dependent on the migration aperture, depth of observation, and dominant wavelength (Chen and Schuster, 1999). A fact often ignored is that the migration aperture limits the maximum dip of structures that can be seen on the migration image; the steeply dipping parts are not imaged (see, e.g., Hertweck et al., 2003 and Toxopeus et al., 2008). Note that illumination and resolution on the migration image can be analyzed efficiently using ray tracing (Lecomte, 2006). Additional limitations worth mentioning are the neglect of converted waves and anisotropy. Locally converted shear waves influence the reflection response as a function of angle of a stack of thin layers (Simmons and Backus, 1994). Anisotropy in the overburden can also influence this response (Wright, 1987).

In this section, we give special attention to two further problems of standard inversion: the effects of averaging reflection coefficients over specular reflection angle θ and of pulse distortion on the migration image varying with reflector dip angle β. These angles are indicated in the upper-left portion of Figure 1 and in Figure 2, respectively. In our examples, we restrict ourselves to primary unconverted P-wave reflections in a 2.5D setting. In such a setting, point sources and 3D spreading are used but the medium does not vary in the direction perpendicular to the plane containing the sources and receivers (Bleistein et al., 2001).

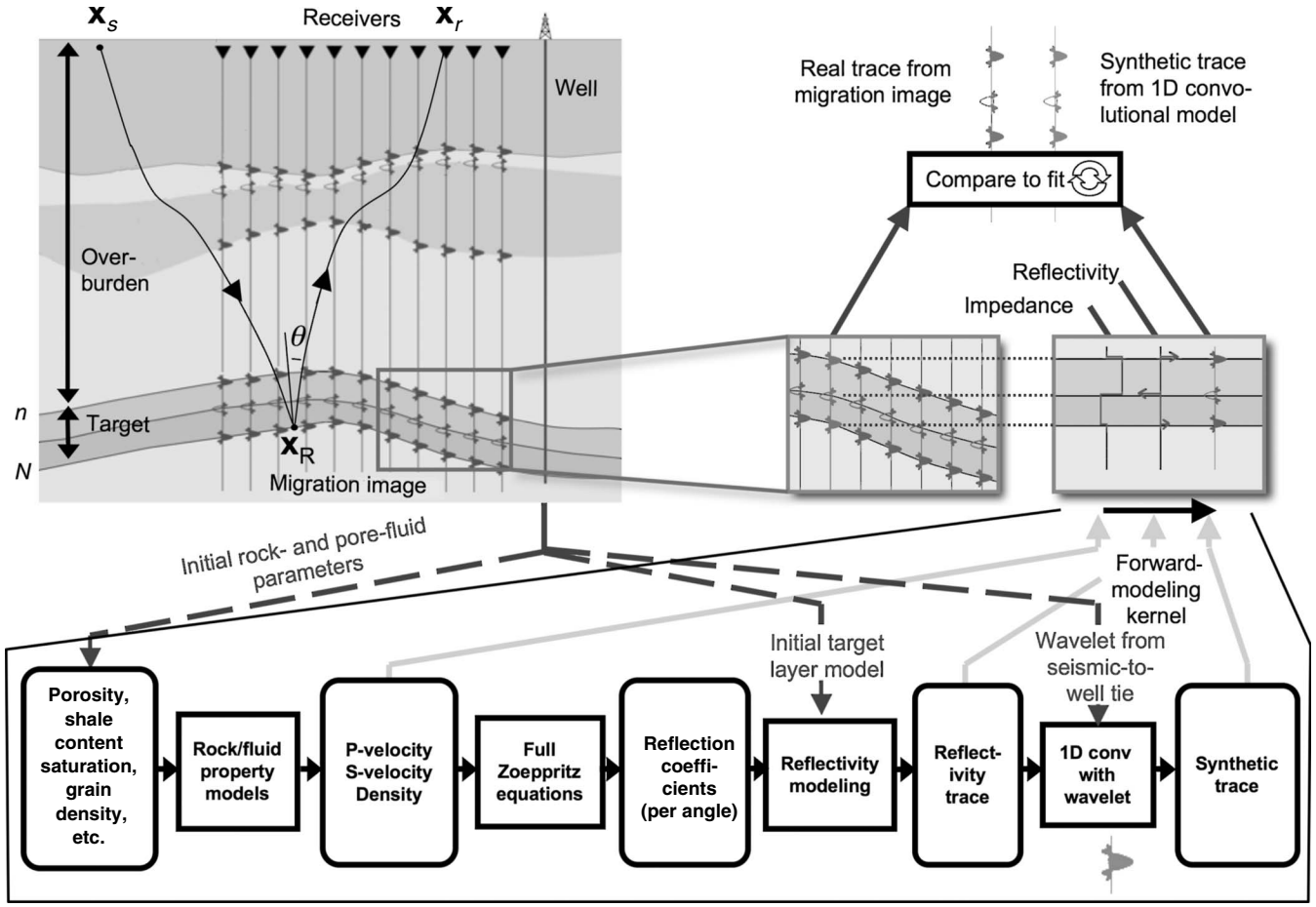

Figure 1. Overview of conventional trace inversion with detailed forward-modeling stage.

Downloaded 21 Sep 2009 to 145.94.65.141. Redistribution subject to SEG license or copyright; see Terms of Use at http://segdl.org/

Averaging over reflection angle θ

A shortcoming of standard inversion that we suspect to be harmful for reservoir parameter estimation in a laterally strongly variable subsurface is that the migration image in practice is a band-limited image of angle-averaged reflection coefficients $\bar{R}(\bar{\theta})$, yet usually $R(\theta = 0)$ is assumed when constructing $r(t)$ for 1D convolution (or when $\theta \neq 0$, a horizontally layered model is used to compute θ). We do not investigate this effect in our paper (see van der Burg [2007] for a brief analysis), but our new inversion scheme properly takes into account θ by means of ray tracing.

Wavelet stretch induced by reflector dip β

On the migration image, wavelet distortion inevitably occurs (Black et al., 1993; Brown, 1994; Tygel et al., 1994), whereas in the inversion the wavelet, $w(t)$ is assumed stationary. This has an impact on parameter estimation in a reservoir with strong structural dip variations.

Theory

Wavelet distortion is a consequence of varying reflection angle θ, reflector dip β, and/or P-wave propagation velocity V_P. The governing expression that measures wavelet stretch in a 2.5D setting along the vertical direction is (Tygel et al., 1994)

$$m_0(V_P,\theta,\beta) = \frac{2}{V_P}\cos\theta\cos\beta, \tag{2}$$

with m_0 denoting the ratio between the wavelet length in the two-way recording time domain and the length in the depth domain, $V_P(\mathbf{x})$ the local P-wave velocity, $\theta(\mathbf{x})$ the angle of ray incidence, and $\beta(\mathbf{x})$ the local reflector dip. For blocky velocity models, the stretch-evaluation point $\mathbf{x}$ on the depth-migrated image is chosen just above or below the velocity discontinuity.

For a reflector on a zero-offset depth-migrated image, the stretch induced by a reflector dip β_0 at position $\mathbf{x}_A$, relative to the stretch at point $\mathbf{x}_B$ with zero dip, is

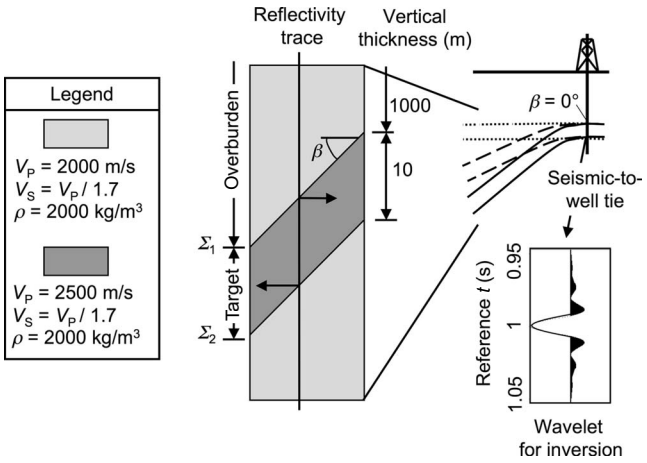

Figure 2. Model of a structure with flank dipping at angle β and a well at zero dip. The single contrasting thin layer has V_P=2500 m/s and h = 10 m. For our tests, $\theta = 0$.

$$n_0'(\beta_0) = \frac{m_0(V_P(\mathbf{x}_B),\theta=0,\beta=0)}{m_0(V_P(\mathbf{x}_A),\theta=0,\beta=\beta_0)} = \frac{V_P(\mathbf{x}_A)}{V_P(\mathbf{x}_B)}\frac{1}{\cos\beta_0}. \tag{3}$$

Inversion is performed usually after 1D depth-to-vertical two-way time conversion of the depth-migrated data. In this procedure, a scaling of the migration image along the vertical with local velocity occurs (see equation 13), effectively removing the velocity dependency in the stretch equation above. This yields the expression for the dip-dependent migration-induced wavelet stretch $n_0(\beta)$ on the depth-to-vertical time-converted zero-offset migrated image:

$$n_0(\beta) = \frac{1}{\cos\beta}. \tag{4}$$

In practice, this means the wavelet representing the position of a reflector on the migration image in vertical two-way time is stretched more with increasing reflector dip. As pointed out by Levin (1998), the display of the migration image with vertical traces causes this stretch. In our new ray-based inversion method, we ensure the inversion occurs in a frame oriented perpendicular to the layering in the reservoir zone by incorporating reflector-oriented ray tracing.

Numerical test: Effect on conventional inversion

To analyze the effect of migration wavelet stretch $n_0(\beta)$ on the inversion of traces from the migration image, consider the following simple but illustrative example: A series of synthetic data tests was performed in a 2.5D normal-incidence ($\theta = 0$) setting using the model depicted in Figure 2. The experiments involve standard inversion for layer properties V_P and h ($< \lambda_d$, the dominant wavelength) using the wavelet derived at $\beta = 0$ on a single trace from a set of ideal migration images shown in Figure 3, each corresponding to a flank with a different dip. (In ideal migration images, all migration artifacts besides wavelet stretch are suppressed, described in detail later.)

The normal-incidence data set was characterized by a Hanning-tapered zero-phase band-pass wavelet with corner frequencies of 4–12–50–75 Hz. In the experiments, exact mean values and the position of Σ_1 (the upper boundary of the layer) were supplied to the inversion as prior knowledge. Figure 4 gives the layer V_P and h estimates for the various dip angles. For higher dip angles, inversion results clearly deviate considerably more than two standard deviations from the desired values.

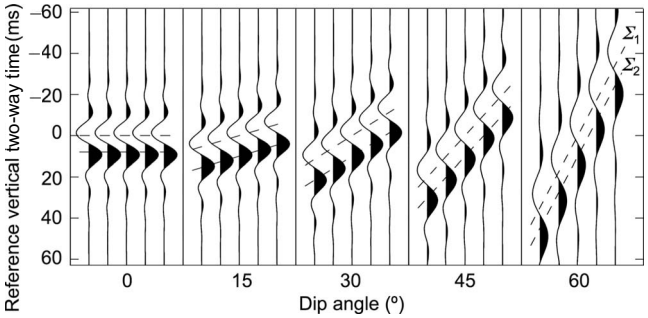

Figure 3. Migration-induced dip-dependent wavelet stretch $n_0(\beta)$ on a detail of ideal migration results for the subsurface model of Figure 2 with dip angle as indicated. Trace separation is 10 m. Dashed lines denote contrasts Σ_i.

Downloaded 21 Sep 2009 to 145.94.65.141. Redistribution subject to SEG license or copyright; see Terms of Use at http://segdl.org/

In the next section, we present our unique inversion method, which inverts in the prestack unmigrated domain and therefore is unaffected by migration stretch.

RAY-BASED STOCHASTIC INVERSION

To compute uncertainties in a laterally variable subsurface, specular reflection-angle and raypath information is needed to determine the local reflection coefficient. We propose incorporating this information inside the inversion by replacing the 1D convolutional model with 3D dynamic ray tracing in a stochastic inversion scheme (Figure 5). To emphasize the evaluation along raypaths, the new inversion scheme is called ray-based stochastic inversion (van der Burg et al., 2004), detailed in van der Burg (2007). In the following, we refer to it as the ray-based or new method as opposed to standard stochastic trace inversion, which we refer to as the conventional or old method.

Earlier efforts have been made in prestack inversion for reservoir characterization using ray theory. Smith and Gidlow (1987) use ray tracing through 1D models to compute reflection angles in common-midpoint (CMP) gathers, whereas in our method ray tracing can be performed in a 3D laterally strongly varying subsurface. Also, there has been a renewed effort to retrieve elastic parameters of the subsurface from prestack data using full waveform inversion (Mora, 1987, 1989; Pratt, 1999; Pratt and Shipp, 1999). Unlike these methods, which concentrate on retrieving the elastic parameters on large to medium scales, our approach inverts for a large range of reservoir rock and pore-fluid parameters on the reservoir scale at target level. Another important difference is that the approaches mentioned above are deterministic inversions that do not give the uncertainty estimates in the results obtained with our method.

Because we are using dynamic ray tracing, we neglect (as in conventional stochastic inversion) the effect of the locally converted shear wave or, alternatively, we assume its effects can be removed in preprocessing. Also, it is good to note that the result of the stochastic inversion depends on the quality of the prior information.

Principle

For ray-based inversion, the subsurface is parameterized as an overburden macromodel overlying a layered target reservoir and is assumed to satisfy the standard ray-theoretical validity conditions (Červený, 2001). The reservoir is identified by a clearly distinguishable reference reflector. Instead of 1D convolution, the new method uses 3D dynamic ray tracing in the forward-modeling kernel.

Concentrating on unconverted, primary P-wave reflections, the key vehicle for ray-based inversion is formed by a single pair of P-wave rays leaving the specular reflection point $\mathbf{x}_R$ on the reference reflector at angles θ to the normal vector $\hat{\mathbf{n}}(\mathbf{x}_R)$ and arriving at the source and receiver positions $\mathbf{x}_s$ and $\mathbf{x}_r$, respectively, at the surface (see Figure 1).

Layer parameters in the inversion target are updated iteratively using a guided Monte Carlo algorithm. The new method minimizes the mismatch between the target reflection response—forward modeled by 3D dynamic ray tracing to the layer interfaces in the target—and the real recordings from the prestack unmigrated data. The modeled response is defined uniquely by the source-receiver pair $(\mathbf{x}_s,\mathbf{x}_r)$, the initial directions (θ,ϕ) (measured from $\hat{\mathbf{n}}(\mathbf{x}_R)$ in the plane of propagation at angle ϕ with the azimuth), the velocity model $V_P(\mathbf{x})$, and the source wavelet.

Simplification: Inversion along normal-incidence rays

If we restrict ourselves to $R(\theta = 0)$, the inversion is performed on the normal-incidence gather. For the practical advantage of reducing data overhead, we also restrict ourselves to a 2.5D setting. In the overburden, 3D dynamic normal-incidence ray tracing is performed to the reference reflector to find those source/receiver locations of the survey that contain reflection information from the reservoir and to calculate overburden amplitude effects. In the target, 1D convolution is used to model the target reflection response on the normal-incidence gather after preprocessing to compensate for the overburden amplitude effects. The flow chart is depicted in Figure 6.

Transmission and spreading effects in the target are not modeled by 1D convolution. However, as long as the target interval behaves locally as a stack of plane-parallel layers, contains a moderate number of layers with impedance contrasts that are not too large, and has a total interval thickness of a few dominant wavelengths at most, the error will be negligible (van der Burg, 2007). The 1D convolutional

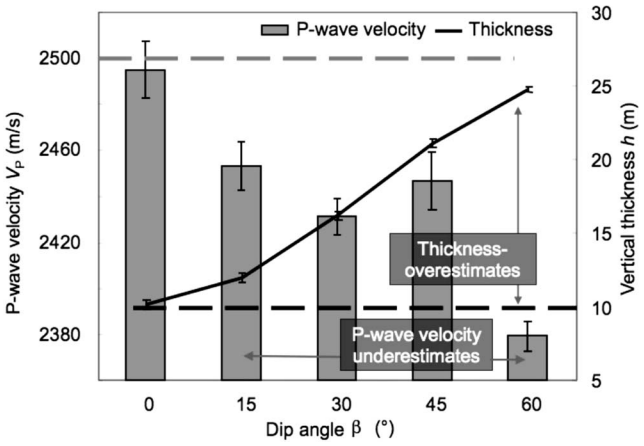

Figure 4. Estimates of V_P and h from standard inversion for the dips indicated on the horizontal axis. Error bars denote posterior standard deviations. Dashed horizontal lines denote desired values for V_P (gray) and h (black).

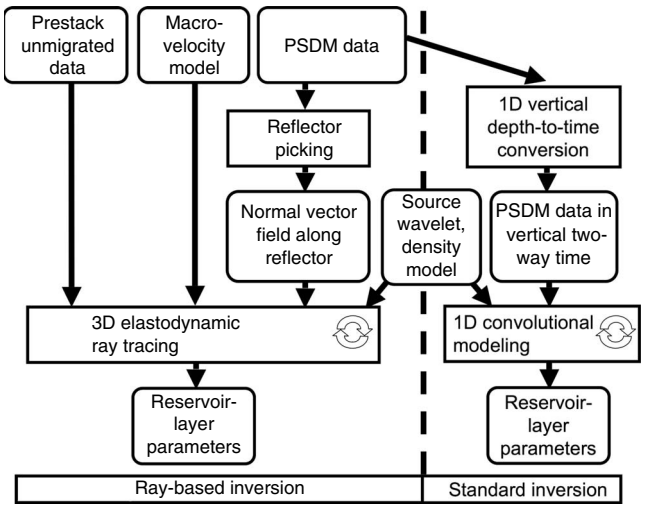

Figure 5. Flow chart for the new ray-based inversion (left) and the standard method (right). The new scheme uses 3D ray-based modeling and is applied to prestack unmigrated data. PSDM = prestack depth migrated.

Downloaded 21 Sep 2009 to 145.94.65.141. Redistribution subject to SEG license or copyright; see Terms of Use at http://segdl.org/

kernel offers a practical advantage because it is readily available in common inversion software. The simplified method, called 1D convolutional ray-based stochastic inversion, is introduced in van der Burg et al. (2005).

Theory

Consider a 2.5D setting with a caustic-free isotropic-elastic subsurface consisting of an inhomogeneous overburden overlying a set of $N-n$ plane-parallel layers (Figure 1). The isotropic point source is $S(\mathbf{x},t)=w(t)\delta(\mathbf{x}-\mathbf{x}_s)$, with $w(t)$ denoting the real-valued wavelet, assuming normalized source strength. The dip angle of the package of layers in the target is β, and vertical thicknesses are $h_i<\lambda_d$, with λ_d the dominant wavelength. Real thicknesses are $h_i'=h_i\cos\beta$. The overburden P-velocity and density macromodels are assumed to be known.

For the chosen configuration, the vertical component of the particle-displacement vector measured from an unconverted primary P-wave normal-incidence reflection at a reflection point $\mathbf{x}_R$ on the lowest interface in the target Σ_N using ray theory can be written as

$$u_3(\mathbf{x}_s=\mathbf{x}_r,\mathbf{x}_R;t)=U_3^{(0)}(\mathbf{x}_s=\mathbf{x}_r,\mathbf{x}_R)w(t-\tau(\mathbf{x}_s=\mathbf{x}_r,\mathbf{x}_R)), \tag{5}$$

with $U_3^{(0)}$ denoting the real-valued amplitude function of the vertical component of the vectorial particle displacement. The wavelet is placed at τ, the normal-incidence two-way traveltime to reflection point $\mathbf{x}_R$. The expression on the right-hand side of equation 5 represents the leading term of the formal asymptotic ray-series expansion solution of the general elastodynamic wave equation.

The amplitude function $U_3^{(0)}$ can be calculated using the expression

$$\begin{aligned}U_3^{(0)}(\mathbf{x}_s=\mathbf{x}_r,\mathbf{x}_R)&=C_B(\mathbf{x}_s,\mathbf{x}_T)R(\mathbf{x}_R,\theta=0)\\&\times T_N(\mathbf{x}_s=\mathbf{x}_r)[\mathcal{L}_B(\mathbf{x}_s,\mathbf{x}_T)\\&+\mathcal{L}_T(\mathbf{x}_T,\mathbf{x}_R)]^{-1},\end{aligned} \tag{6}$$

with $\mathbf{x}_T$ being the intersection point of the normal-incidence ray with interface Σ_n, dividing the raypath in parts through the overburden and the target. The overburden amplitude effects are denoted by C_B, which are caused by transmission through interfaces and the presence of a free surface. The expression $R(\theta=0)$ is the normal-incidence Zoeppritz reflection coefficient measured from the ray-incidence direction, and $T_N=\Pi_{i=n}^{N-1}T_i^-(\theta=0)T_i^+(\theta=0)$ is the product of transmission losses in the target (while the ray pair crosses $N-n$ interfaces through the target: $N>n$ and $n\geq 1$; for $n=1$, the overburden does not contain interfaces). Finally, $\mathcal{L}$ is the relative geometric spreading as defined in Červený (2001). It includes the effects of reflector curvature.

The zero-offset particle-displacement data set $u_3(\mathbf{x}_s=\mathbf{x}_r,\mathbf{x}_R;t)$ is preprocessed so that all overburden amplitude effects caused by C_B and $\mathcal{L}_B$ are removed, i.e.,

$$\begin{aligned}U_{3,\mathrm{prep}}^{(0)}(\mathbf{x}_s=\mathbf{x}_r,\mathbf{x}_R)&=\left[\frac{\mathcal{L}_B}{C_B}\right]U_3^{(0)}(\mathbf{x}_s=\mathbf{x}_r,\mathbf{x}_R)\\&=RT_N\mathcal{L}_B(\mathcal{L}_B+\mathcal{L}_T)^{-1}.\end{aligned} \tag{7}$$

If amplitude losses within the target resulting from T_N and $\mathcal{L}_T$ are neglected (i.e., $T_N\approx 1$ and $\mathcal{L}_T/\mathcal{L}_B\ll 1$), it follows that

$$U_{3,\mathrm{prep}}^{(0)}(\mathbf{x}_s=\mathbf{x}_r,\mathbf{x}_R)\approx R(\mathbf{x}_R,\theta=0), \tag{8}$$

a necessary condition for the application of a 1D convolutional inversion kernel on the data set.

The depth-migrated image is used in the new method to pick the reference reflector indicating the target. Standard inversion operates on traces from the true-amplitude prestack depth-migrated (PSDM) image. It is constructed from the measured vertical component of the particle velocity $\dot{u}_3=\partial u_3/\partial t$ as follows (modified from Schleicher et al., 1993):

$$\begin{aligned}\langle R(\mathbf{x},\theta=0)\rangle\simeq-\frac{2}{\pi}\int\int_{\mathbf{x}_r\in A}&\frac{1}{T(\mathbf{x}_r)C_0(\mathbf{x}_r)}\frac{\partial}{\partial t}\\&\times\dot{u}_3(\mathbf{x}_r;t)_{t=t_d}\mathrm{d}x_{r,1}\mathrm{d}x_{r,2},\end{aligned} \tag{9}$$

in which t_d represents the two-way traveltime between $\mathbf{x}$ and $\mathbf{x}_s=\mathbf{x}_r$, dependent on the P-wave velocity model $V_P(\mathbf{x})$. The time derivative $\partial/\partial t$ operating on $\dot{u}_3$ in the migration equation ensures the phase of the wavelet is preserved on the migration output, i.e., it compensates for the phase-shift effect caused by the double integration (Newman, 1990). The variable T takes into account target and overburden transmission losses, C_0 accounts for the free surface, and $\langle\ \rangle$ denotes that R is spatially band limited.

SYNTHETIC DATA TEST

We compare the new method with conventional inversion for determining V_P and h of the layers from a thin-layered structure that resembles a real data case discussed later. With this synthetic test, we intend to focus on the effect of wavelet stretch; hence, we model only noise-free primary P-wave reflections in the synthetic data.

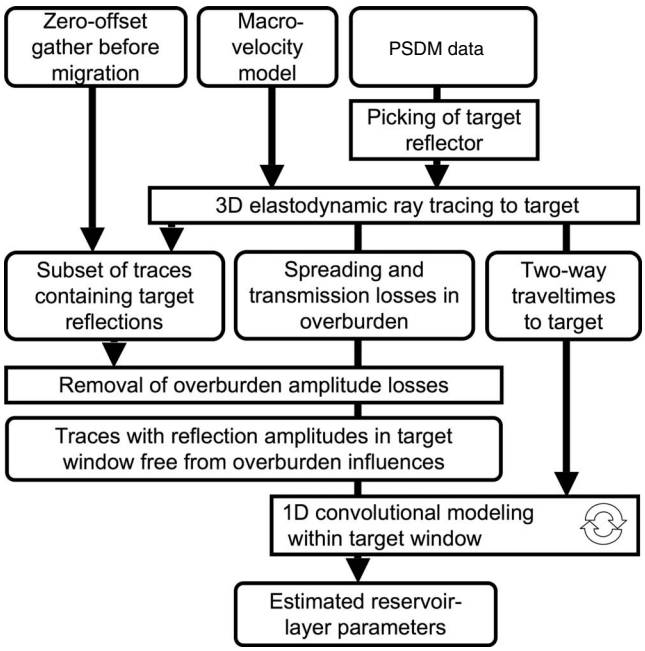

Figure 6. Flow chart for 1D convolutional ray-based inversion. PSDM = prestack depth migrated.

Downloaded 21 Sep 2009 to 145.94.65.141. Redistribution subject to SEG license or copyright; see Terms of Use at http://segdl.org/

Model geometry

The model is depicted in Figure 7. It consists of a target of five thin layers below the sixth interface Σ_6 that serves as the reference reflector and the boundary between overburden and target. Layer properties are invariant in the x_2-direction, so the variations are restricted to the (x_1,x_3)-plane and data acquisition (using point sources and 3D spreading) is performed along the x_1-direction to obtain a 2.5D configuration. Everywhere, the layer S-wave velocity is $V_P/1.7$.

The position of the layer interfaces in the overburden including the target reference reflector Σ_6 is given by the following equation:

$$x_{3,i}(x_1) = x_{3,i}^{\max} - \Delta x_{3,i} \exp \frac{-(x_1-\mu)^2}{2\sigma^2} \qquad (10)$$

for $i \in \{1,2,\ldots,6\}$, with $\sigma = 1000$ m, $\mu = 3000$ m, $\Delta x_{3,i} = x_{3,i}^{\max} - x_{3,i}^{\min}$, where $x_{3,i}^{\max}$ and $x_{3,i}^{\min}$ can be read from Figure 7.

The positions of the five target interfaces below the reference reflector are calculated by applying a simple translation in depth to Σ_6:

$$x_{3,i}(x_1) = x_{3,i-1}(x_1) + h_i \forall\, i \in \{7,8,\ldots,11\}, \qquad (11)$$

with h_i denoting the (laterally constant) vertical layer thicknesses (in meters) in the target, given by $h_i = \{50,8,5,10,7\}$ for $i \in \{7,8,9,10,11\}$. This target configuration is favorable for conventional inversion in the sense that dips β for all target interfaces are the same for a given x_1, which means that the associated dip-dependent migration wavelet stretch $n_0(\beta)$ in the target will be constant per trace from the migrated image. However, the locally plane-parallel layer assumption for the new method is not satisfied fully because dips are not exactly the same along reflector normals.

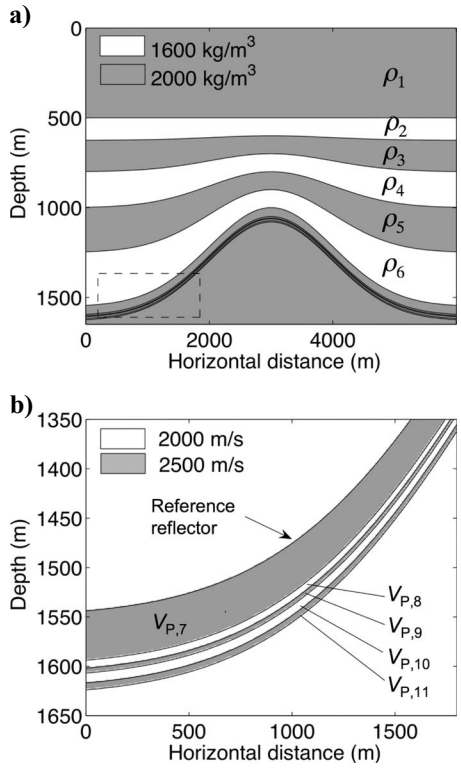

Figure 7. (a) Density distribution. Density in the target is constant at 2000 kg/m^3. (b) Enlargement of the dashed area, showing the P-wave velocity distribution in the target. Overburden velocity is constant at 2000 m/s.

Normal-incidence data set

The normal-incidence data set $\dot{u}_3(\mathbf{x}_s = \mathbf{x}_r;t)$ on which 1D convolutional ray-based inversion will be applied is generated using dynamic ray tracing (equations 5 and 6). It is computed for 601 source-receiver positions with 10-m spacing at the free surface. The data set must be preprocessed before it can be inverted by the new method. The overburden amplitude losses, calculated by dynamic ray tracing to the reference reflector, are removed using equation 7 to compensate for the effect of the laterally varying overburden on target-reflection amplitude.

For the wavelet in equation 5, the zero-phase Gabor wavelet is used (Hubral and Tygel, 1989; their equation 1):

$$w(t) = \cos(2\pi f_d t) e^{-(2\pi f_d t/\gamma)^2}, \qquad (12)$$

with t denoting the two-way traveltime, $f_d = 35$ Hz the dominant frequency, and parameter $\gamma = 4$. Note that at zero dip in the chosen model, the two-way traveltime coincides with vertical two-way traveltime. Thus, equation 12 also applies to the zero-dip wavelet present on the depth-to-time converted migrated image.

Ideal migrated data set

The conventional method inverts traces from the PSDM 1D vertical depth-to-time converted image of the normal-incidence data for layer thickness and P-wave velocity in the target. In this case, it inverts the ideal migrated image to isolate the effect of dip-dependent migration wavelet stretch on conventional inversion; the effects of illumination and limited lateral resolution are absent.

This ideal migration image is generated by first applying a 1D vertical depth-to-time conversion to the model of the elastic properties in depth, using the exact P-wave velocity model:

$$t_v(x_1,x_3) = \int_0^{x_3} \frac{2}{V_P(x_1,x_3')} \mathrm{d}x_3', \qquad (13)$$

with $t_v(x_1,x_3)$ denoting the vertical two-way traveltime corresponding to some depth location $\mathbf{x}$ and $V_P(x_1,x_3)$, the laterally and vertically varying P-velocity. In this way, the exact position of all interfaces in vertical two-way traveltime and the size of the impedance contrasts associated with the interfaces are known.

Next, for every 10 m in the x_1-direction, an acoustic impedance trace is synthesized from the density and P-wave velocity models in vertical two-way traveltime, with which the normal-incidence reflection coefficients are calculated. Subsequently, a spiky reflectivity trace $r(t_v)$ can be computed — the impulse response of a 1D layered earth, considering the earth as a linear system — with the expression (van Riel and Berkhout, 1985; their equation 2)

$$r(t_v) = \sum_{j=1}^{N} R_j \delta(t_v - \tau_j), \qquad (14)$$

with N denoting the number of reflectors, R_j the normal-incidence reflection coefficients, δ Dirac's delta function, and τ_j the lag time of the jth reflector. Finally, $r(t_v)$ is convolved (see equation 1) with a varying dip-dependent wavelet, which has the proper migration

Downloaded 21 Sep 2009 to 145.94.65.141. Redistribution subject to SEG license or copyright; see Terms of Use at http://segdl.org/

wavelet stretch $n_0(\beta)$, depending on the local dips β of the reflectors encountered. The stretch is calculated using equation 4 and applied to the original Gabor wavelet at zero dip.

Inversion: Conventional versus ray based

The inversion goal is to estimate h and V_P for each layer in the target. Ray-based inversion inverts for true thickness h', which afterward is converted to vertical thickness h using the local dip at the reflection points on the top interfaces of the target layers known from ray tracing (van der Burg, 2007). Furthermore, the h and V_P estimates from ray-based inversion found at irregularly distributed reflection points on each target interface are interpolated to a regular lateral interval of 10 m, coinciding with the migration output grid, so a direct comparison with the estimates obtained by conventional inversion can be made.

Prior knowledge

Knowledge of the reservoir before inversion for both types of inversions includes the correct number of target layers; layer-ρ; $V_S = V_P/1.7$; and ρ, V_P, and V_S outside the target. The correct wavelet is assumed to be derived from the normal-incidence section (ray-based inversion) and from the horizontal part of the zero-offset migrated section (conventional inversion).

For all layers, the prior mean $\mu(V_P)$ coincides with the true V_P, whereas the uncertainty is described by a standard deviation of $\sigma(V_P) = 250$ m/s. For all h (and h'), prior mean $\mu(h)$ coincides with true h (and h') with an uncertainty described by a standard deviation of $\sigma(h) = 5$ m for the first (thick) target layer and $\sigma(h) = 1$ m for the other target layers. The normal distributions were bounded at a minimum value of zero; during the stochastic inversion, samples drawn outside this bound were rejected. The two-way traveltime to the reference reflector was known up to a standard deviation of 2 ms.

Inversion results

The posterior reservoir models obtained from standard and ray-based inversions are depicted in Figure 8. To facilitate the observation of the thickness estimates, the estimated reservoir model is displayed after flattening along the reference reflector and showing only a portion of the bottom of the first target layer. Also, for improved display, a six-point moving-average filter is applied on the h and V_P estimates for each layer in the lateral direction. The filter width is equal to the lateral resolution at target level on the migration image.

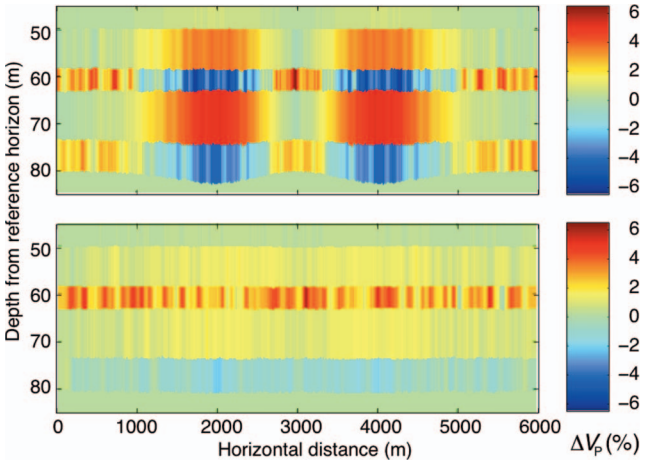

Figure 8. Reservoir model as found by conventional inversion (top) and 1D convolutional ray-based inversion (bottom) flattened along the reference reflector. Colors indicate V_P misestimates. Notice the h overestimates for the conventional method at the dipping parts.

Layer thicknesses clearly are overestimated by the old method in the parts of the reservoir that have strong dips. In contrast, the thickness estimates from the new method do not suffer from this overestimation. The V_P estimates for the simplified method are closer to the desired values as well, although errors increase for the lower layers because of the neglect of spreading and transmission losses in the target. Posterior standard deviations (not shown) do not differ much with this noise-free data.

FIELD DATA TEST

We tested 1D convolutional ray-based inversion and compared it with conventional inversion using a real data set from the Gulf of Mexico (courtesy Shell Offshore Inc., New Orleans, U.S.A.). The deepwater Gulf of Mexico field in which the inversion tests are done is a hydrocarbon-bearing reservoir consisting of sheet sands and shales. The reservoir contains a horizontal and dipping part with dips up to 31° (see Figure 9). The test strategy is depicted in Figure 9. For a fair comparison, both methods perform a seismic-to-well tie at the same calibration well on a horizontal part of the target, and both use the same prior information.

Based on results from synthetic tests, we suspect the artifacts caused by migration deteriorate the standard inversion results in the dipping part of the reservoir. This is verified by checking the inversion results with the logs of an evaluation well drilled right through the slope after the initial inversion was complete, representing a blind test. The comparison in this field data test is complicated by remaining multiple energy, locally converted shear waves, and anisotropy. None of these effects is taken into account in old or new methods. The presence of noise and uncertainties in the prior information of the wavelet are additional complications in the comparison. For initial test descriptions, see van der Burg et al. (2007).

Seismic data description

A 3D high-resolution seismic survey was conducted over the area. The seismic data were recorded in an acquisition campaign that was

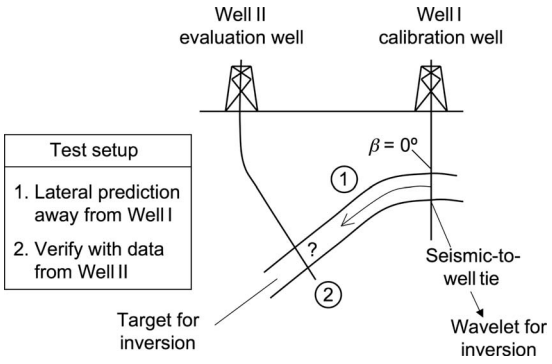

Figure 9. The capabilities in lateral prediction of target reservoir parameters away from well I (the exploration well) to the dipping part of the target at well II are tested for conventional versus ray-based inversion.

Downloaded 21 Sep 2009 to 145.94.65.141. Redistribution subject to SEG license or copyright; see Terms of Use at http://segdl.org/

a follow-up of a previous 3D seismic survey. It was deployed to support well placement, reduce uncertainty, and allow prestack interpretation. To succeed in these goals, a very large, usable signal bandwidth of up to 80 Hz was needed. The desired high-frequency preservation and structural detail required a fine spatial sampling at the surface of 6.25 m inline $\times$12.5 m crossline (later interpolated to 6.25 m) and a temporal sampling of 2 ms.

Because the geometry of the target was known from the previous survey, the acquisition configuration could be optimized by sailing the marine acquisition vessel approximately in dip lines over the target (see Figure 10).

Processing before migration

To prepare the data for true-amplitude PSDM, Shell applied preprocessing in which the relative amplitude behavior of target interface reflections was preserved as much as possible. The most important process was a 3D normal moveout/dip moveout (NMO/DMO)—inverse NMO/DMO sequence. There were two reasons for this. First, we wanted to obtain an early structural image of the target via prestack time migration before applying the computationally expensive true-amplitude PSDM. Second, it suppresses acquisition footprints and regularizes data. During the inverse DMO, an offset depopulation was done from 80 to 48 offsets, with output offsets ranging from 450 to 6325 m and with a 125-m offset increment.

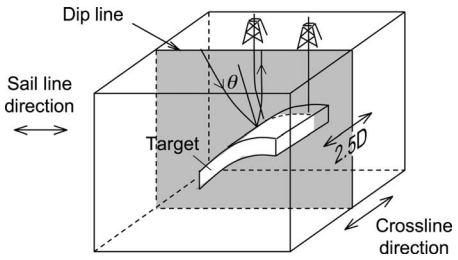

Figure 10. Dip line in a 3D seismic data cube. Around this sail line, the subsurface is assumed laterally invariant in the crossline direction. A specular ray pair is shown on the top interface of the target with reflection angle θ.

The left side of Figure 11 depicts a portion of the 575-m common-offset gather for the dip-line selected for inversion. The reflectors around 4000 ms on the right side of this gather mark the target for inversion. Also visible are some diffractions, mainly from the overburden, and a reflection-triplication caused by the convex shape of the reflectors. On these high-quality data, prestack interpretation is attainable, and prestack inversion should be feasible.

True-amplitude PSDM

A common-offset true-amplitude prestack P-wave Kirchhoff depth migration (Schleicher et al., 1993) was applied on the offset gathers from the preprocessed prestack data using the P-wave velocity model obtained from velocity analysis during a preceding prestack time migration and traveltime inversion. This velocity model was defined on a grid with an inline/crossline/depth spacing of 100 m. The migration operator grid was sampled twice as densely, with a spacing of 50 m.

The migrated data were available in vertical two-way traveltime, directly suitable for conventional inversion. The prestack unmigrated data had to be downsampled from 2 to 4 ms two-way traveltime to obtain a manageable data size for migration; 4 ms is also the output sampling in vertical two-way time after migration. The spatial output sampling in the inline and crossline directions was 12.5 m — twice the size of the inline midpoint distance.

After prestack migration, a stack was made for the 16 nearest offsets from 450 to 2325 m to increase the signal-to-noise ratio and facilitate structural interpretation. Before inversion, a phase rotation of 90° was applied to the image, an operation sometimes applied to improve the interpretation of inversion results in the target. In Figure 11 (middle), a portion of the near-stack migrated section along the dip line is displayed.

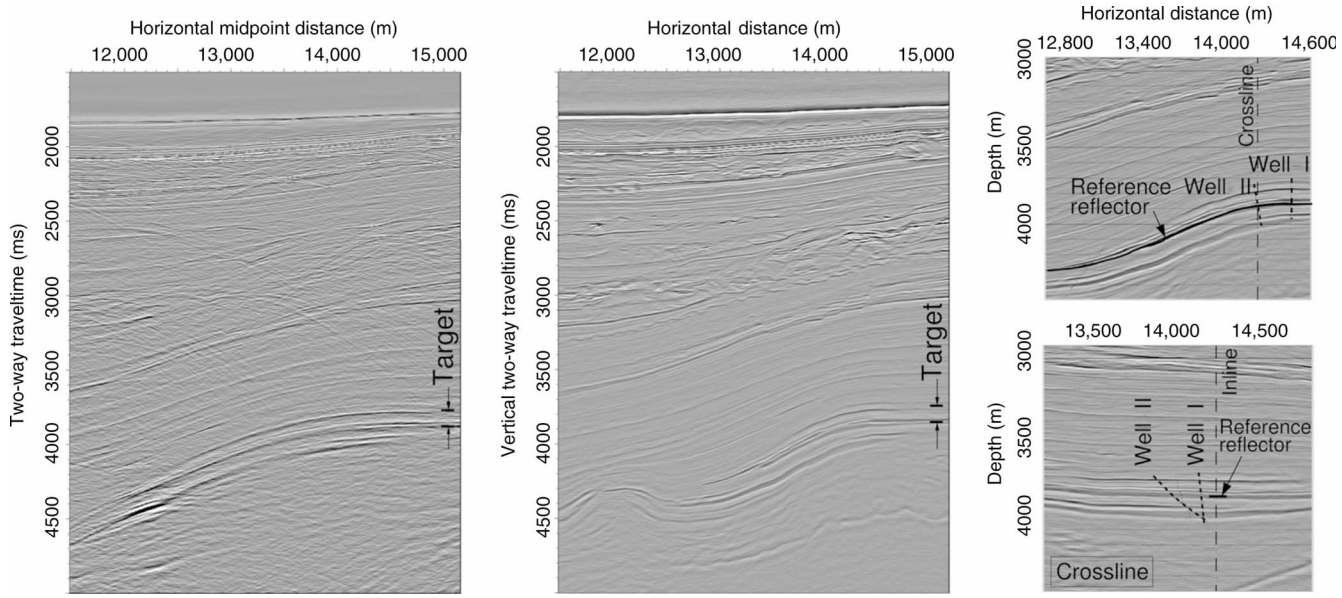

Figure 11. Portion of the 575-m common-offset gather (left) and the near-stack migrated image (middle) along the dip line. The rightmost two panels indicate well paths projected on the migrated image in depth, inline (top), and crossline.

Downloaded 21 Sep 2009 to 145.94.65.141. Redistribution subject to SEG license or copyright; see Terms of Use at http://segdl.org/

Seismic data selection for inversion

The selection (from the total data volume) of the migrated and prestack unmigrated data to be inverted is performed on the basis of three criteria: conformity to a 2.5D setting, proximity of wells, and data quality. Although no fundamental limitations exist that prevent applying 1D convolutional ray-based inversion in a 3D setting, the comparative tests against conventional inversion are performed in a 2.5D setting to reduce data overhead by confining the analysis to the migrated and prestack unmigrated data along a single sail line.

On the right side of Figure 11, two paths of wells traversing the target are displayed in the inline and crossline directions. The crossline is taken at the point where well II intersects the reference reflector. It shows that the inline is not placed ideally but is close enough to wells I and II, taking into account that the target seems to remain approximately laterally constant (2.5D) in the crossline direction between the sail line and well II.

For the prestack data, the gather for the first available offset (450 m) suffered significantly more from high-frequency noise around the target zone at 4000 ms than the next offset gather (575 m), so the latter was preferred for ray-based inversion.

Model geometry

The reservoir model consists of a sequence of seven layers situated directly above the reference horizon. It is a subset from a larger sequence of layers originally used for conventional inversion; the subset meets the application requirements for 1D convolutional ray-based inversion. The inversion interval was chosen to extend laterally from the horizontal part at 15,100 m to the steepest part at 13,800 m horizontal distance, where dip increases to a maximum of 31°. The total thickness is about 100 m, with layer rock types alternating between shale and sand-shale mixture.

To describe the relationship between the rock properties of the shaly sandstone reservoir rocks typically encountered in the Gulf of Mexico and the elastic properties ρ, V_P, and V_S, shale and laminated sandstone-shale rock models are used. These models take advantage of property trends derived from well logs (see van der Burg, 2007, for details). The reservoir-rock parameters inverted for are P-wave velocity V_P, vertical thickness h, and sand fraction SF. Here, we concentrate on V_P and h. Gaussian distributions of these parameters are assumed.

Conventional inversion

In the first part of the comparative test, standard inversion is used to invert the stacked migrated image for the unknown reservoir-layer parameters. A seismic-to-well match is done to derive the wavelet from the migrated data using the detailed log information present at well I, the first drilled well vertically penetrating the horizontal part of the target. The top of Figure 12 shows the migrated data around this well and the derived wavelet.

The prior mean values $\mu(V_P)$ and standard deviations $\sigma(V_P)$ are displayed, after flattening along the reference reflector, on the left side of Figure 15, which summarizes the results of the old and new methods. Prior $\mu(h)$ can be inferred from the interface positions; $\mu(SF)$ is laterally constant.

Posterior $\mu(V_P)$, $\sigma(V_P)$, and $\mu(h)$ are depicted in the center of Figure 15. The seemingly rapid lateral changes in layer thicknesses result from the chosen way of plotting with much vertical exaggeration. Posterior $\sigma(V_P)$ are mostly smaller than the prior $\sigma(V_P)$, indicating an inversion convergence. Notice that a five-point moving-average filter was applied on the results obtained for the separate traces. In choosing the filter width, care was taken not to smooth more than the lateral resolution at target level on the migration image.

1D convolutional ray-based inversion

In the second part of the comparative test, the new simplified method is used to invert the prestack near-offset section for the unknown reservoir-layer parameters.

Prestack seismic data selection

To select from the 575-m common-offset gather those source-receiver pairs that contain reflection information on the specified inversion target, ray tracing is done to the reference reflector in the migration P-wave velocity model. In the process, the two-way traveltimes to the reference reflector are calculated; these are required for tying the inversion window to the traces.

The ray tracing is performed in a 2.5D setting with the source-receiver pairs on the dip line and no crossline subsurface property variations. Source-receiver distance is set to 575 m, and separation between midpoints is 6.25 m to mimic the acquisition configuration of the real data. Figure 13 shows every tenth ray. The angles of incidence are up to $\theta = 6°$.

When forward modeling the portion of the offset gather containing the target reflection response, the small additional traveltimes in the target caused by $\theta \neq 0°$ will be neglected, whereas the actual ray-incidence angles are taken into account when computing the reflection coefficients. The reference reflector is a mildly smoothed ver-

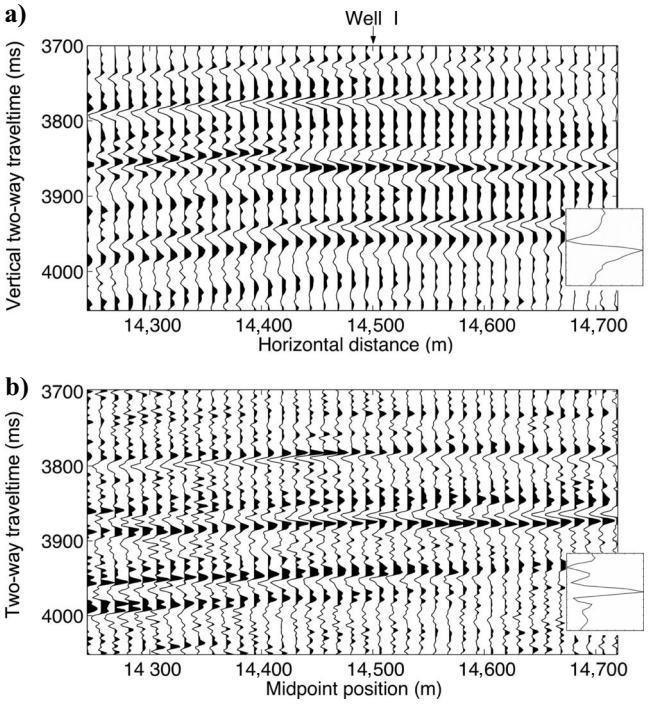

Figure 12. Good data quality on target level around well I on (a) the migrated substack and (b) the 575-m common-offset gather, containing more high-frequency information. Insets show 100 ms of derived wavelets; a 90° phase rotation was applied to the migrated data.

Downloaded 21 Sep 2009 to 145.94.65.141. Redistribution subject to SEG license or copyright; see Terms of Use at http://segdl.org/

sion from the original handpicked interface, which still fits the true reflector quite well as seen from the near-stack migration image in the background. Also, the migration velocity model was smoothed in a trade-off between kinematic accuracy and dynamic stability (van der Burg, 2007).

Figure 13 also shows a range of source-receiver pairs that has more than one reflection point on the reference reflector. This is the reflection-triplication mentioned earlier. For practical convenience, this area is avoided. Dealing with multivaluedness in principle can be incorporated into the forward-modeling kernel of ray-based inversion. The chosen reflection-point range is indicated with an arrow along the reference reflector. The corresponding midpoint range is 12,700–15,100 m, which includes the vertical well at 14,500 m. Finally, the box indicates part of the reservoir (enlargements are shown in Figure 14).

The lower panel of Figure 12 shows the area around the vertical well on the 575-m common-offset gather and the wavelet derived for ray-based inversion. For practical reasons, the derivation neglects the spherical spreading and transmission losses in the reservoir zone,

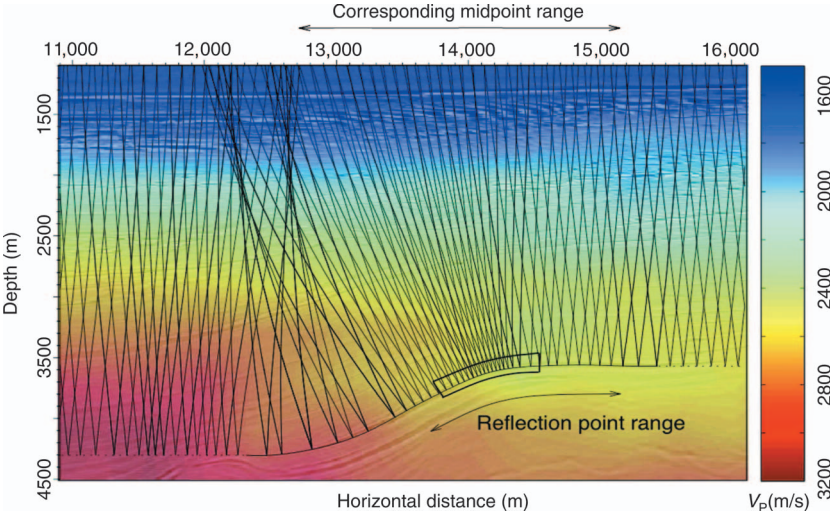

Figure 13. Rays to the reference reflector in the migration velocity model; migration image is shown in the background.

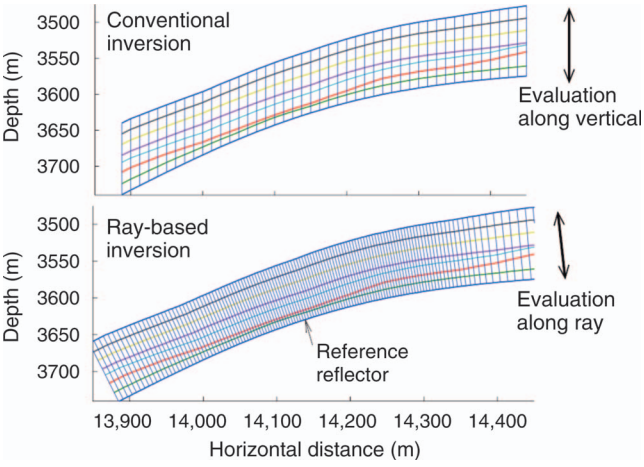

Figure 14. Enlargement of the boxed area in Figure 13, showing the different evaluation directions and plotted with the prior layer positions from each method.

the small extra traveltime in the target from having small-offset data while assuming zero offset, and the slightly different reflection coefficients for small nonzero angles of incidence at the reflector.

Transforming the prior model from conventional inversion

For ray-based inversion, the layer properties and thicknesses must be specified along the raypath, which generally does not correspond to the vertical direction along which conventional inversion is operating. Figure 14 shows the situation for a portion of the reservoir model marked with a box in Figure 13.

To obtain the prior model for the new method, a dip-dependent conversion of the prior model for conventional inversion must be done. This conversion assumes that the target satisfies the application regime of 1D convolutional ray-based inversion. As a consequence of the plane-parallel layering assumption, normal-incidence raypaths to the reference reflector are assumed to be straight through the inversion target. The layer properties are evaluated along these normal-incidence rays, starting from the reflection points on the reference reflector (see also van der Burg, 2007; Figure 5.25).

Overburden amplitude correction

Dynamic ray tracing through the migration velocity model to the reference horizon also yields the laterally varying overburden effects $C_B/\mathcal{L}_B$ needed for preprocessing the prestack unmigrated data in 1D convolutional ray-based inversion.

The medium under the reference reflector is chosen as a homogeneous half-space with known elastic properties. With the medium properties above the reflector also specified by the model, the Zoeppritz unconverted P-wave reflection coefficient $R(\theta)$ at the reference reflector (with $\theta \approx 6°$) is known exactly and can be divided out, leaving the desired overburden amplitude effects $C_B/\mathcal{L}_B$ in the calculated amplitudes.

In the final amplitude correction applied to the traces from the common-offset gather, amplitude variations faster than the lateral resolution on the migration image were smoothed using an eighth-degree polynomial fit.

Inversion results

After resampling to the grid used by standard inversion and applying a five-point moving-average filter, the V_P and h estimates are shown on the right side of Figure 15. Notice the decreased total package thickness compared to the conventional method, a result expected for the dipping part of the reservoir where the conventional method suffers from wavelet stretch. The anomalous depressions with a peak in between, in the rightmost part of the reservoir above 14,800 m, correspond to a portion of low data quality on the offset gather.

From these observations, one should realize that the only place where a quantitative judgment of the inversion results can be made is at the well location. This is the subject of the next section.

Downloaded 21 Sep 2009 to 145.94.65.141. Redistribution subject to SEG license or copyright; see Terms of Use at http://segdl.org/

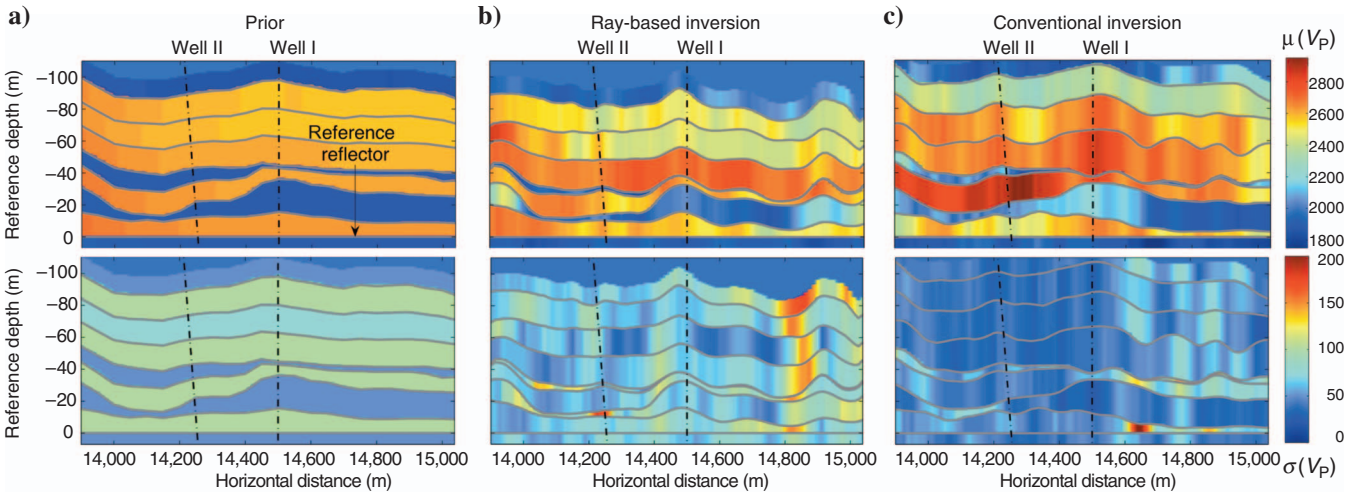

Figure 15. Overview of prior model (a) and posteriors for ray-based (b) and conventional (c) inversion. Colors indicate V_P (m/s); mean values are displayed on top, standard deviations below. For a clearer display, flattening is done along the reference reflector, and the vertical scale is exaggerated.

Comparison at well II

In the third part of the comparative test, the inversion results obtained with the old and new methods are compared with the values found at well II (Figure 16). From the column of target layers, the sandstone-shale mixture layers (underburden [UDB], 2, 4, and overburden [OVB]) are discerned easily using the gamma-ray and sonic logs because of their high sand fraction. In the area around well II, it is more difficult to discern sand-shale mixture layer 6 because of its low sand fraction and, consequently, its low contrast with the surrounding shale layers. Additional trends from the neutron log were needed. After interpretation, the average P-wave velocity per layer was determined from the blocked sonic log.

Figure 16 shows that the conventional method generally overestimates layer thicknesses, whereas the 1D convolutional ray-based inversion estimates are slightly better, with the values from well II within one standard deviation from the estimated means. However, for thin layers 2 and 4, the estimated thicknesses from the old method are better (but overestimated). The V_P estimates are closer to the actual values using the new method.

Standard deviations are higher for the new method resulting from the higher amount of noise on the offset gather compared to the near-stack migrated section. However, the philosophy for full ray-based inversion is to reduce these standard deviations by adding more measurements (offset gathers) into the inversion. Here, only one of 48 offsets was used. Moreover, an estimate with a larger standard deviation does not necessarily have to be worse. For example, for the P-wave velocity estimates of layer 2, the means are estimated about the same. However, conventional inversion gives a misleadingly small standard deviation; the true value falls well outside the error bar.

The total package thickness of 86.5 m at well II is overestimated by the old method, as predicted by theory, to 99 ± 3.5 m. The new method somewhat underestimates the package thickness but remains within one standard deviation from the true value of 81±6.5 m.

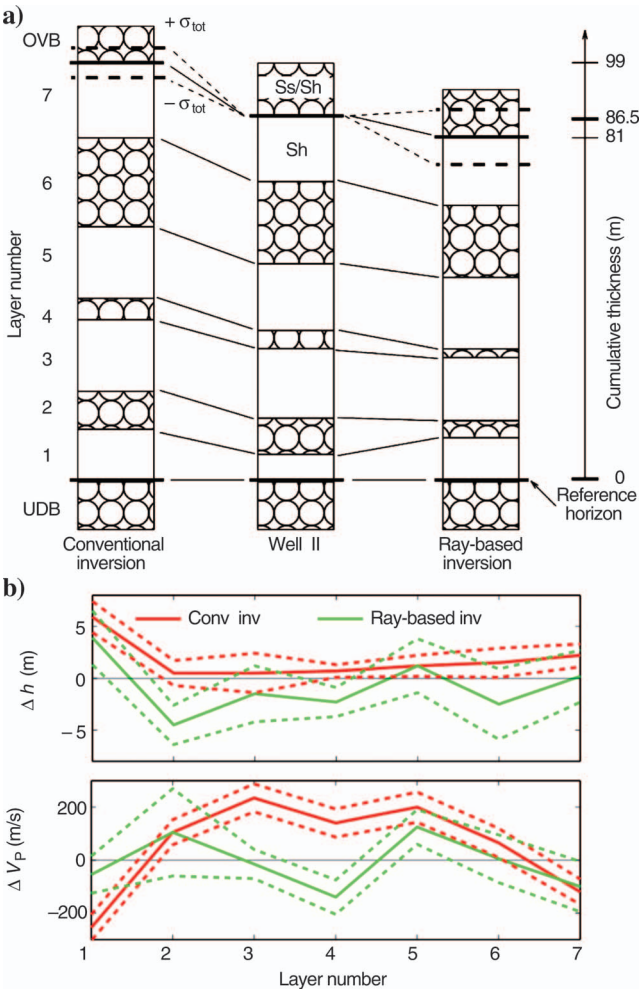

Figure 16. (a) Rock column, showing true and estimated mean vertical thickness h of the shale (Sh) and sand-shale mixture (Ss/Sh) layers at well II, with standard deviations for total h. UDB=underburden; OVB=overburden. (b) Misestimates in h and P-wave velocity V_P, including standard deviations (dashed). Red curves are conventional inversions; green curves are ray-based inversions.

Downloaded 21 Sep 2009 to 145.94.65.141. Redistribution subject to SEG license or copyright; see Terms of Use at http://segdl.org/

CONCLUSIONS

Our new method for reservoir parameter estimation inverts prestack seismic reflection data before migration using stochastic inversion along raypaths. The novelty in the technique is the combination of ray tracing and stochastic inversion to use the original wavepath and reflection-angle information contained in the prestack data to estimate reservoir parameters, including uncertainties. It has become feasible to use ray tracing in a computationally intensive stochastic scheme because of the increased processing power of computers and the computational speed and efficiency of the ray method. The new ray-based stochastic method can be applied to estimate reservoir parameters in a structurally complex subsurface with substantial lateral velocity variations and significant reflector dips.

Synthetic data tests show the distortion of the wavelet in the seismic migration image as a function of reflector dip and reflection angle is an important effect that is not taken into account by conventional trace-inversion techniques. The new method operates in the prestack unmigrated domain; therefore, it is unaffected by this migration-induced wavelet stretch.

The prestack data before migration that are inverted by the new method contain the original angle-dependent reflection information needed for a good inversion for reservoir parameters. On the contrary, conventional trace inversion techniques operate on migrated (sub)stacks where angle-dependent reflection information is sacrificed for a better signal-to-noise ratio with respect to reflector positioning.

When applied to normal-incidence data, the new method inverts along raypaths that are perpendicular to the reflectors, the direction that offers optimal resolution for discerning the layering in the reservoir assuming an isotropic subsurface and unconverted primary P-waves.

Obviously, the lateral resolution on the prestack data before migration is not as good as on migrated data that are focused, but the loss of resolution can be compensated in several ways, e.g., by accurate modeling of edge diffractions.

In its current implementation, the forward modeler of the new method only handles isotropic subsurfaces and primary P-wave reflections. A future study should investigate the impact on the inversion results of anisotropy in the overburden and converted shear waves. A more robust extension of the method could then include such effects in forward modeling.

Results from the Gulf of Mexico field data study show that the thickness and P-wave velocity estimates obtained with the simplified new method are better than those obtained with conventional inversion, in the sense that the new estimates are more often within one standard deviation from the desired values. Hence, a good result can be obtained by working properly with a tiny fraction of the data. Only 2% of the available prestack data were used with 1D convolutional ray-based inversion. However, we expect that adding multioffset data would constrain the inversion operation better.

It would be interesting to investigate the potential of reusing rays calculated on the diffraction grid for preserved-amplitude Kirchhoff migration in ray-based stochastic inversion to save computing time and to interweave inversion with migration.

ACKNOWLEDGMENTS

The authors wish to thank Shell International E&P B.V. for supporting this research financially and for permission to publish this work. The field data set was made available by Shell Offshore Inc. The reviewers are thanked kindly for their suggestions to improve the paper. We are indebted to Paul Gary (Shell E&P Co.) and Jaap Leguijt (Shell International E&P B.V.) for their continuous support in acquiring and inverting the field data.

REFERENCES

Black, J. L., K. L. Schleicher, and L. Zhang, 1993, True-amplitude imaging and dip moveout: Geophysics, **58**, 47–66.
Bleistein, N., J. Cohen, and J. Stockwell Jr., 2001, Mathematics of multidimensional seismic imaging, migration, and inversion: Springer.
Brown, R., 1994, Image quality depends on your point of view: The Leading Edge, **13**, 669–673.
Červený, V., 2001, Seismic ray theory: Cambridge University Press.
Chen, J., and G. T. Schuster, 1999, Resolution limits of migrated images: Geophysics, **64**, 1046–1053.
Duijndam, A. J. W., 1987, Detailed Bayesian inversion of seismic data: Ph.D. dissertation, Delft University of Technology.
Hertweck, T., C. Jäger, A. Goertz, and J. Schleicher, 2003, Aperture effects in 2.5D Kirchhoff migration: A geometrical explanation: Geophysics, **68**, 1673–1684.
Hubral, P., and M. Tygel, 1989, Analysis of the Rayleigh pulse (short note): Geophysics, **54**, 654–658.
Lecomte, I., 2006, Illumination, resolution, and incidence-angle in PSDM: A tutorial: 76th Annual International Meeting, SEG, Expanded Abstracts, 2544–2548.
Leguijt, J., 2001, A promising approach to subsurface information integration: 63rd Annual Conference and Exhibition, EAGE, Extended Abstracts, L35.
Levin, S. A., 1998, Resolution in seismic imaging: Is it all a matter of perspective?: Geophysics, **63**, 743–749.
Mora, P., 1987, Nonlinear two-dimensional elastic inversion of multioffset seismic data: Geophysics, **52**, 1211–1228.
———, 1989, Inversion = migration + tomography: Geophysics, **54**, 1575–1586.
Newman, P., 1990, Amplitude and phase properties of a digital migration process: First Break, **8**, 397–403.
Oldenburg, D. W., T. Scheuer, and S. Levy, 1983, Recovery of the acoustic impedance from reflection seismograms: Geophysics, **48**, 1318–1337.
Pratt, R. G., 1999, Seismic waveform inversion in the frequency domain, Part 1: Theory and verification in a physical scale model: Geophysics, **64**, 888–901.
Pratt, R. G., and R. M. Shipp, 1999, Seismic waveform inversion in the frequency domain, Part 2: Fault delineation in sediments using crosshole data: Geophysics, **64**, 902–914.
Sambridge, M., and K. Mosegaard, 2002, Monte Carlo methods in geophysical inverse problems: Reviews of Geophysics, **40**, 1–29.
Schleicher, J., M. Tygel, and P. Hubral, 1993, 3-D true-amplitude finite-offset migration: Geophysics, **58**, 1112–1126.
Simmons, J. L., and M. M. Backus, 1994, AVO modeling and the locally converted shear wave: Geophysics, **59**, 1237–1248.
Smith, G. C., and P. M. Gidlow, 1987, Weighted stacking for rock property estimation and detection of gas: Geophysical Prospecting, **35**, 993–1014.
Tarantola, A., 2005, Inverse problem theory and methods for model parameter estimation: Society for Industrial and Applied Mathematics.
Toxopeus, G., J. Thorbecke, K. Wapenaar, S. Petersen, E. Slob, and J. Fokkema, 2008, Simulating migrated and inverted seismic data by filtering a geologic model: Geophysics, **73**, no. 2, T1–T10.
Tygel, M., J. Schleicher, and P. Hubral, 1994, Pulse distortion in depth migration: Geophysics, **59**, 1561–1569.
van der Burg, D. W., 2007, Ray-based stochastic inversion of pre-stack seismic data for improved reservoir characterisation: Ph.D. dissertation, Delft University of Technology.
van der Burg, D., A. Verdel, and K. Wapenaar, 2004, Ray-based stochastic inversion: 74th Annual International Meeting, SEG, Expanded Abstracts, 1607–1610.
———, 2005, Ray-based stochastic inversion for reservoir parameters using 1D convolutional forward modeling: 75th Annual International Meeting, SEG, Expanded Abstracts, 1441–1444.
———, 2007, Ray-based stochastic inversion: Improving reservoir characterization in a Gulf of Mexico field: 77th Annual International Meeting, SEG, Expanded Abstracts, 1775–1779.
van Riel, P., and A. J. Berkhout, 1985, Resolution in seismic trace inversion

Downloaded 21 Sep 2009 to 145.94.65.141. Redistribution subject to SEG license or copyright; see Terms of Use at http://segdl.org/

by parameter estimation: Geophysics, **50**, 1440–1455.
Veeken, P. C. H., and M. Da Silva, 2004, Seismic inversion methods and some of their constraints: First Break, **22**, 47–70.
White, R., and R. Simm, 2003, Good practice in well ties: First Break, **21**, 75–83.
Wright, J., 1987, The effects of transverse isotropy on reflection amplitude versus offset (short note): Geophysics, **52**, 564–567.
Young, G. B., and L. W. Braile, 1976, A computer program for the application of Zoeppritz's amplitude equations and Knott's energy equations: Bulletin of the Seismological Society of America, **66**, 1881–1885.

Downloaded 21 Sep 2009 to 145.94.65.141. Redistribution subject to SEG license or copyright; see Terms of Use at http://segdl.org/